Journal of Molecular Liquids 357 (2022) 119104

Contents lists available at ScienceDirect

Journal of Molecular Liquids

journal homepage: www.elsevier.com/locate/molliq

Surface functionalization of graphene oxide with tannic acid: Covalent vs non-covalent approaches

Carlos Sainz-Urruela, Soledad Vera-López, María Paz San Andrés, Ana M. Díez-Pascual *

Universidad de Alcalá, Facultad de Ciencias, Departamento de Química Analítica, Química Física e Ingeniería Química, Ctra. Madrid-Barcelona Km. 33.6, 28805 Alcalá de Henares, Madrid, Spain

ARTICLE INFO

Article history:
Received 4 March 2022
Revised 2 April 2022
Accepted 5 April 2022
Available online 08 April 2022

Keywords:
Surface functionalization
Tannic acid
Graphene oxide
Bioactive compound
Covalent grafting

ABSTRACT

Graphene oxide (GO) is gaining a lot of interest in material science, biomedicine and biotechnology due to its outstanding physical properties, combined with its surface functionalization capacity, processability in aqueous media and biocompatibility. However, van der Waals forces among GO layers result in aggregation, yet its dispersion, large-scale production, and reinforcing efficiency remain challenging. Herein, simple and environmentally friendly methods via covalent and non-covalent routes have been developed to exfoliate and prepare surface-functionalized GO nanosheets with tannic acid (TA), a biological macromolecule with antioxidant activity. Four esterification strategies were tested: direct, carbodiimide activated, oxalyl chloride acylation and via an acid-functionalized GO intermediate. The resulting samples have been extensively characterized to get knowledge on the GO-TA interactions and the degree of grafting, as well as their surface topography, level of hydrophilicity, solubility/dispersibility, thermal and antibacterial properties. The covalent grafting of TA renders the GO surface more hydrophobic, resulting in improved dispersion in organic solvents. Besides, TA acts as a crosslinker between the GO nanosheets, leading to higher thermal resistance. A synergistic effect of both GO and TA on inhibiting bacterial growth has also been found. The esterification via carbodiimide leads to the highest grafting degree, the best thermal stability and the most effective antibacterial activity. This work not only highlights the great potential of TA for both exfoliation and surface functionalization of GO, but also extends its applications in biomedicine and for the development of green nanocomposites.

© 2022 The Authors. Published by Elsevier B.V. This is an open access article under the CC BY-NC-ND license (http://creativecommons.org/licenses/by-nc-nd/4.0/).

1. Introduction

Graphene oxide (GO) is now gaining significant relevance owed to its exceptional properties, which render it appropriate for a comprehensive range of applications like energy, biomedicine, biotechnology, polymer composites and so forth [1–5]. It comprises oxygenated functional moieties, mainly carboxyl, carbonyl, epoxy and hydroxyl, as well as other minor groups including lactone and quinone. These functional groups present on GO are polar, making it very hydrophilic and partially water-soluble, being its degree of solubility dependent on the C/O ratio [6]. Thus, it is straightforward exfoliated in water solutions with the application of ultrasounds, yielding colloidal dispersions with long-term stability, resulting in improved processability in aqueous media. Furthermore, it offers easiness of synthesis, surface functionalization capacity, excellent antibacterial properties [7] and it is biocompatible, hence is a suitable alternative to pristine graphene.

This nanomaterial can be functionalized via covalent and non-covalent modifications in order to form derivatives with improved properties [8]. Covalent functionalization can be easily accomplished in aqueous solution via anchoring of organic molecules to the oxygenated groups onto the GO surface. Due to the rich chemistry of oxygenated groups, GO is very reactive, particularly with nucleophiles. In this regard, conjugated polymers [9], organic chromophores such as porphyrins [10], phthalocyanines, and azobenzene and other organic molecules like octadecylamine [11], butylamine [12], phenyl isocyanate [13] and so forth have been covalently linked to GO. Such modifications maintain the GO 2D lattice; however, they modify the π-conjugated electronic cloud located above and below the graphenic sheet, leading to significant modifications in its properties. Nonetheless, nucleophilic reduction reactions generally prevail over functionalization, hence GO reactions typically yield reduced graphene oxide (rGO) with low functionalization degree [14].

In contrast, the non-covalent strategy relies on the physical adsorption and/or enfolding by molecules or polymers through hydrogen-bonding, van der Waals and other weak interactions like

* Corresponding author.
E-mail address: am.diez@uah.es (A.M. Díez-Pascual).

https://doi.org/10.1016/j.molliq.2022.119104
0167-7322/© 2022 The Authors. Published by Elsevier B.V.
This is an open access article under the CC BY-NC-ND license (http://creativecommons.org/licenses/by-nc-nd/4.0/).

H − π, π–π, cation − π, and anion − π, which preserve the electronic characteristics of GO [8]. Non-covalent GO functionalization with nucleic acids [15], surfactants [16] and end-terminated polymers [7] has been reported. This strategy has some advantages over the covalent route: (i) it is developed under mild conditions (aqueous media at ambient temperature), which conserves the aromatic structure and prevents spoilage of the GO nanosheets; (ii) the procedure allows controlling the adsorbed/wrapped amount, which is difficult to do via chemical reaction.

Tannic acid (TA) is a polyphenol found in nature that can be taken from different parts (i.e. stem, leaf) of plant species as well as twigs, bark or wood of certain trees including Chestnut and Oak [17]. It has valuable biological and pharmacological properties such as antioxidant, antibacterial, antiallergenic, and anticarcinogenic ability as well as biodegradability [18]. The combination of high bioactivity, abundance in nature, inexpensiveness and outstanding biocompatibility make this tannin appropriate for food supplements, leather manufacturing, biomedical and biological industries, etc. Owed to its complexation capability with other molecules, TA was traditionally applied for treatment of diseases like diarrhea or digestive disorders and topically to wear skin burns. Besides, it has been recognized to be successful for the treatment of ulcers [19].

In terms of chemical structure, TA comprises a central glucose molecule joined to 10 gallic acids through ester moieties. Plentiful neighboring phenolic hydroxyls and ester moieties render high chemical reactivity, hence it can react with numerous molecules by means of covalent and non-covalent interactions (i.e. van der Waals, hydrophobic, π-π), and metal–organic coordination interactions [20,21]. Moreover, it contains 25 hydroxyl groups that account for its weak acidity and numerous hydrogen bonds. However, different pKa data for TA have been published, lately 6.4, 7.5, and 8.6 [22] and it can be oxidized in basic medium.

The synthesis of graphene-based nanomaterials usually encompasses toxic and corrosive acids that are detrimental to the environment and human health. Recently, rGOs have been prepared via a single stage reductive process using green biomolecules such as dopamine, gallic acid, caffeic acid, and tea polyphenol [23–26]. These natural compounds not merely act as reducing agents but also as stabilizers, thus preventing the aggregation of GO nanosheets and promoting their dispersion in aqueous solutions, resulting in composites with easier processability and improved performance. Similarly, TA is a strong natural reducing agent due to its antioxidant activity. The reduction of GO by polyphenols like TA has been proposed to involve two steps [27]: firstly, a phenolic hydroxyl group of the polyphenol attacks an epoxy group on GO, generating an adjacent new hydroxyl; secondly, this new hydroxyl is attacked by another phenolic hydroxyl. The resulting intermediate undergoes an elimination reaction leading to a conjugate bond at the initial epoxy site while the phenolic groups transform into diquinone.

In this regard, a few articles dealing with GO and TA materials for different applications have been published over latest years. Singhal *et al.* [28] developed superhydrophilic GO membranes crosslinked with TA using a simple and cost-effective vacuum filtration methodology for efficient treatment of oil-contaminated water. Akkya and coworkers [29] reported the preparation of an electrochemical biosensor for glucose sensing based on a glassy carbon electrode modified with a TA-reduced GO nanocomposite and Pt nanoparticles. Simultaneous reduction of GO and Pt^{4+} was performed in a simple and low-cost way using TA, which can reduce both oxidized carbon materials and metal ions such as gold, silver, iron, etc. [30]. Yao *et al.* [31] synthesized a pH-responsive TA functionalized graphene hydrogel by random copolymerization of 2-acrylamido-2-methyl-1-propane sulfonic acid and acrylic acid in the presence of TA-rGO, which shows great potential as an adsorbent for cationic dyes. Similarly, Tang *et al.* [32] developed TA-GO hydrogels via a one-step hydrothermal method that could effectively address the problems of low adsorption capacity in water purification. All the abovementioned articles are based on a reversible redox reaction between GO and TA. However, to the best of our knowledge, there is no previous study dealing with the functionalization of GO with TA through non-covalent interactions and/or chemical grafting routes. Chemical modification of GO with varieties of functionalities is crucial for anticipated applications such as sensing and composite materials.

In the current work, GO functionalized by TA has been prepared for the first time via non-covalent and covalent strategies. The anchoring of TA onto the GO surface was carried out following four different approaches: direct esterification, carbodiimide-activated, via oxalyl chloride acylation and through preparation of an acid-functionalized GO intermediate. The resulting samples have been thoroughly characterized by different techniques and compared with pristine GO in order to obtain knowledge on the interactions between the two compounds and the extent of the functionalization processes as well as their morphology, level of hydrophilicity, solubility/dispersibility, thermal and antibacterial properties. This study shows the great potential of TA for both exfoliation and surface functionalization of GO. The novel approaches described herein are simple, environmentally friendly and cost-effective procedures for synthesizing highly dispersed functionalized GO nanosheets for use in diverse fields, in particular in biomedicine, for sensor applications or for the development of green antibacterial nanocomposites.

2. Experimental section

2.1. Reagents

Graphene oxide (GO), with 70 μm lateral dimension, 400 m^2/g specific surface area, average thickness of 1–2 nm and oxygen content of 32%, was supplied by Avanzare Innovación Tecnológica S.L. (La Rioja, Spain). Tannic acid (TA > 99.9%, $C_{76}H_{52}O_{46}$, M_w = 1701.2 g/mol), oxalyl chloride (>99.0%, $C_2Cl_2O_2$, M_w = 126.9 g/mol $d_{20°C}$ = 1.50 g/cm^3), chloroacetic acid (>99.0%, $C_2H_3ClO_2$, M_w = 94.5-g/mol, $d_{20°C}$ = 1.58 g/cm^3), and 1-(3-Dimethylaminopropyl)-3-ethyl carbodiimide (EDC, >97.0%, $C_8H_{17}N_3$ M_w = 94.5 g/mol $d_{20°C}$ = 0.877 g/cm^3) were acquired from Sigma Aldrich (Madrid, Spain). Sodium hydroxide, hydrochloric acid and methanol were provided by Panreac Química S.L.U. (Castellar del Vallès, Spain). Phosphate buffer solution was prepared by mixing the stock standard solutions of Na_2HPO_4 (99%) and NaH_2PO_4 (99%), provided by Merck. All dispersions were prepared using ultra-pure water obtained in a Milli-Q system from Millipore (Milford, CT, USA).

2.2. Instrumentation

Dispersions were prepared using an Elmasonic S40 ultrasound bath (Elma Schmidbauer GmbH, Singen, Germany), and were centrifuged using a Digicen 21 centrifuge (OrtoAlresa, Madrid, Spain). Stirring of the mixtures was performed with a magnetic microstirrer (Velp Scientifica, Usmate Velate, Italy). Filtration was carried out with 0.2 μm PTFE membrane filters (Ø = 47 mm, Sartorius AG, Göttingen, Germany).

Solubility/dispersibility tests were carried out in water and in the following organic solvents: methanol, dimethyl sulfoxide (DMSO), ethanol, *N,N*-dimethylformamide (DMF), propanol, acetone, tetrahydrofuran (THF), N-methyl-2-pyrrolidone (NMP), ethylene glycol (EG), toluene, chloroform (CH_3Cl), n-hexane and n-pentane. About 0.5 mg of the sample were mixed with ~ 1 mL solvent and agitated for 10 min with a magnetic stirrer. To assess the

dispersibility, samples were placed in an ice bath and subjected to 10 min ultrasonication with a titanium sonotrode (3 mm diameter). The stability of the dispersion was assessed by means of visual observation of phase separation or sedimentation over one week.

Scanning electron microscopy (SEM) analysis was performed with a Digital Scanning Microscope DSM-950 (Carl Zeiss, Germany) equipped with a tungsten filament as electron source, working under vacuum at 20 kV. Prior to observation, samples were dried out and sputtered with a thin gold layer to avoid charging during electron irradiation. Examination of the micrographs was accomplished with the ImageJ software.

Fourier-transformed infrared (FT-IR) spectra were acquired at 25 °C in the MIR region (500–4000 cm^{-1}) with a resolution of 4 cm^{-1} using a Frontier infrared spectrophotometer (Spectrum Two, Waltham, MA, USA) working in ATR mode.

Room temperature Raman spectra were acquired using a high performance inVia confocal Raman instrument (Renishaw, Gloucestershire, UK) fitted with a Nd:YAG 532 nm laser. Five scans were at least recorded for each compound at a power of 500 mW. The acquisition of data was controlled with Windows®-based Raman Environment software v.2.3. Baseline correction method was applied to remove the baseline drift caused by fluorescence.

Water contact angle experiments were performed at 25 °C with a Model 200 Goniometer (Ramé-hart, USA) equipped with an automated dispensing system. An ultrapure water droplet was situated on the surface of each compound and its growth was captured via CCD camera. The contact angle was calculated using Dropimage Standard v2.3 software. Five droplets were formed on each sample and the mean value is reported.

The thermal stability was assessed via thermogravimetric analysis (TGA) experiments performed under a nitrogen atmosphere at a heating rate of 10 °C/min. Data from 100 to 650 °C were collected with a TA-Q500 thermobalance (TA Instruments, Barcelona, Spain) coupled to a mass spectrometer, and analyzed using TA Universal Analysis software.

The bactericide activity was monitored against Gram-positive *S. Aureus* and Gram-negative *E. coli* microorganisms. Sterilized samples were subsequently immersed in a 72 h old media (comprising beef extract and peptone) of $\sim 1.7 \times 10^6$ CFU/mL. Viable colonies were reckoned subsequently incubation for 1 day at 37 °C using a colony counter. Percentage reduction in bacterial number was calculated using the equation:

$$Bacterial\ \ inhibition(\%) = [(N_r - N_s)/N_s] \times 100 \quad (1)$$

where N_s and N_r are the number of CFU of the tested sample and a reference without sample taken as control, respectively.

2.3. Procedure

2.3.1. Non-covalent modification of graphene oxide with tannic acid

The non-covalent modification was carried out in slightly basic medium (pH = 8.0), so that most of the phenolic groups of TA are protonated (pK_a values of 6.3, 7.4, and 8.6 [22]), hence can form strong hydrogen bonds with oxygenated moieties of GO. In a typical experiment, 5 mg of GO was added to 10 mL of 0.1 M phosphate buffer solution, and the resulting dispersion was ultrasonicated at ambient temperature and 240 Hz for 30 min. Subsequently, 20 mg of TA was slowly added to the GO dispersion and the mixture was subjected to stirring for 1 day (**Figure S1**). The resulting product (GO coated with tannic acid, GO-TA) was obtained by filtering through a PTFE membrane filter, and subsequently thoroughly washed with ultrapure water. The GO-TA was washed thoroughly with ethanol and finally dried under vacuum overnight at 50 °C. An illustration of the non-covalent functionalization route, showing the H-bonding interactions between oxygenated functional groups of GO and the hydroxyl groups of TA, as well as π-π stacking interactions among their aromatic rings, is depicted in Scheme 1.

2.3.2. Covalent modification of graphene oxide with tannic acid

Covalent modification was carried out following four different procedures. In the first approach, pristine GO was directly esterified with TA in acid medium. Firstly, 10 mg of GO was suspended in deionized water (10 mL), gently stirred and maintained at 80 °C under nitrogen for 24 h (**Figure S2**). Then, the GO dispersion was acidified with HCl (pH = 4.7), 20 mg of TA were slowly added and subsequently agitated for 24 h at 80 °C. The resulting nanomaterial (GO-g-TA) was filtered, subjected to several washing cycles and dried under vacuum at 50 °C. The initial bluish-black color of the reactant mixture became darker black once the reaction finished (Figure S2), corroborating the reduction of GO, since rGO color is darker than that of pristine GO [33]. As depicted in Scheme 2, the reaction between epoxy or carboxylic acid moieties of GO with hydroxyl groups of TA would lead to the formation of ether and ester linkages, respectively, together with the removal of water.

A second approach was performed via preparation of acid-functionalized GO (GO-COOH) as intermediate, which was prepared by activating the GO sample with $C_2H_3ClO_2$ in a basic medium to transform the hydroxyl and epoxy groups to carboxylic acid moieties [31]. Typically, 10 mg of GO, 250 mg of $C_2H_3ClO_2$ and 200 mg of NaOH in DI water were mixed and ultrasonicated for 1 h, followed by agitation at RT for 24 h. The resulting GO–COOH suspension was neutralized by HCl, washed with DI water and ethanol several times, and dried overnight at 60 °C. A schematic representation of the GO-COOH synthesis is shown in Scheme 3. The GO-COOH was then grafted to the phenolic groups of TA via esterification reaction, following similar procedure to that mentioned above for GO-g-TA. Henceforth, the obtained compound will be designated as GO-COOH-g-TA-1.

In a third experiment, GO-COOH (10 mg) was suspended in aqueous solution and ultrasonicated for 30 min. Then, 20 mg of TA was added and sonicated for another 30 min. EDC (100 mg) was then added and the mixture agitated under ambient temperature for 1 day. The resulting mixture was coagulated in ethanol. After 1 h of centrifugation and washing thoroughly with DI water and phosphate buffer solution to remove unreacted EDC residues, the product (named as GO-COOH-g-TA-2) was obtained, which was dried at 50 °C under vacuum. A diagram of the synthesis process is depicted in Scheme 4.

The last approach was carried out in two stages, via conversion of the carboxylic acids at the edges of GO nanosheets into acyl chlorides, resulting in the acyl chloride-derivative (GO-CO-Cl) intermediate (Scheme 5). Thus, raw GO (10 mg) was sonicated in DMF (10 mL) for 30 min. After, 20 mL of $C_2Cl_2O_2$ was added to the dispersion under a N_2 atmosphere at 70 °C for 1 day to form GO-CO-Cl. Excess $C_2Cl_2O_2$ was removed through reduced pressure. 20 mg of TA was then added to allow the grafting of TA on GO-CO-Cl for 24 h under nitrogen at 70 °C. The GO-CO-Cl-g-TA product was purified thoroughly by several washing cycles and dried at 60 °C.

3. Results and discussion

3.1. Morphology assessment

SEM was used to analyze the surface topography of the different compounds, and characteristic micrographs are presented in Fig. 1. Pristine GO shows a wrinkled surface topology composed of many flexible nanosheets bound by π–π stacking, polar interactions and van der Waals forces. It consist of fairly thick flakes with thick-

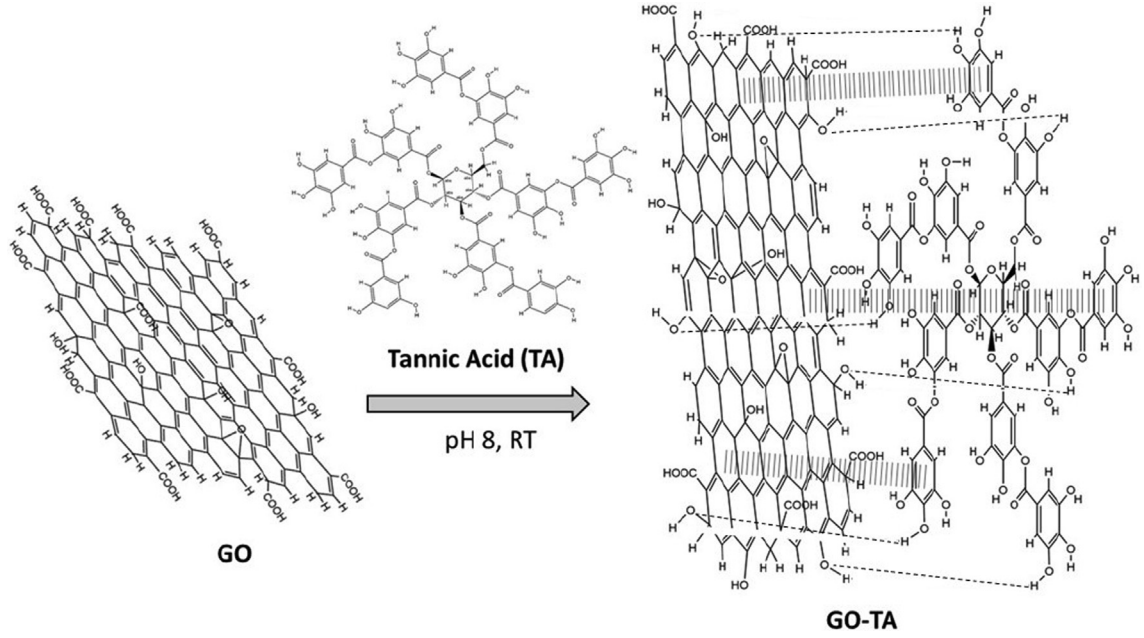

Scheme 1. Scheme of the non-covalent functionalization of GO with TA and the interactions via H-bonding (– – –) and π-π stacking (|||||||).

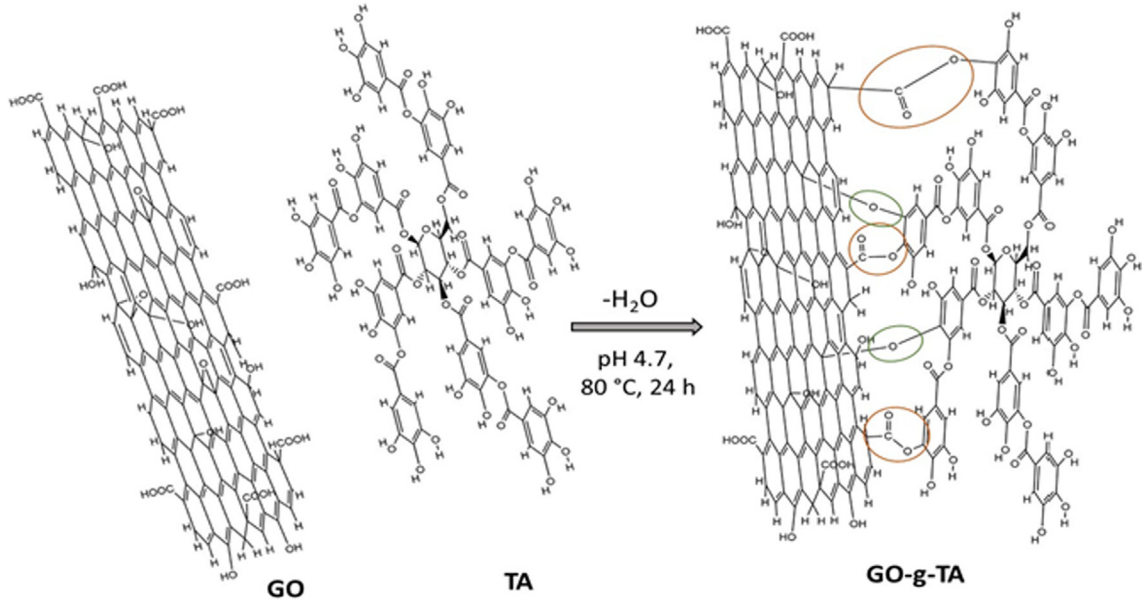

Scheme 2. Illustration of the direct covalent modification of GO with TA via formation of ether (green circles) and ester (red circles) linkages.

nesses in the range of 20–50 nm (Fig. 1a). Despite the thickness of a graphene monolayer should be about 0.35 nm [1], a GO nanosheet is likely considerably thicker due to the oxygenated groups located on both sides of the flakes. These groups expanded the interlayer distance of graphite, and damaged its compact layered microstructure, leading to a wrinkle phenomenon. The sample appears homogeneous and quite aggregated, comprising numerous oxidized graphene layers. It should be noted that some agglomeration can also take place throughout the sample drying to lower surface energy, hence thickness values obtained from the SEM micrographs should be just taken for comparative purposes.

Conversely, the samples with TA seem more heterogeneous. As schematically described in Scheme 1, GO coated with tannic acid (GO-TA) was prepared in one-stage process in a basic aqueous solution. This results in a sample with the TA wrapping around the GO layers, in which a compact stacked structure can be observed (Fig. 1b). The surface foldings are not found in this non-covalently functionalized sample, probable due to the covering effect of the TA molecules that enshroud these wrinkles. Besides, its surface is smoother and coarser than that of pristine GO, with a few discernable defects and increased thickness, up to 70 nm.

Regarding the covalently functionalized samples, a more disentangled and disaggregated structure was found, likely because TA locates in between the GO sheets, thus acting as an exfoliating agent. Besides, it can act as a reducing agent, as indicated by the change in color from bluish-black to darker black during the synthesis of GO-g-TA. Thus, the partially reduced sample (Fig. 1d) exhibits a distinctive morphology with fluffy and more transparent

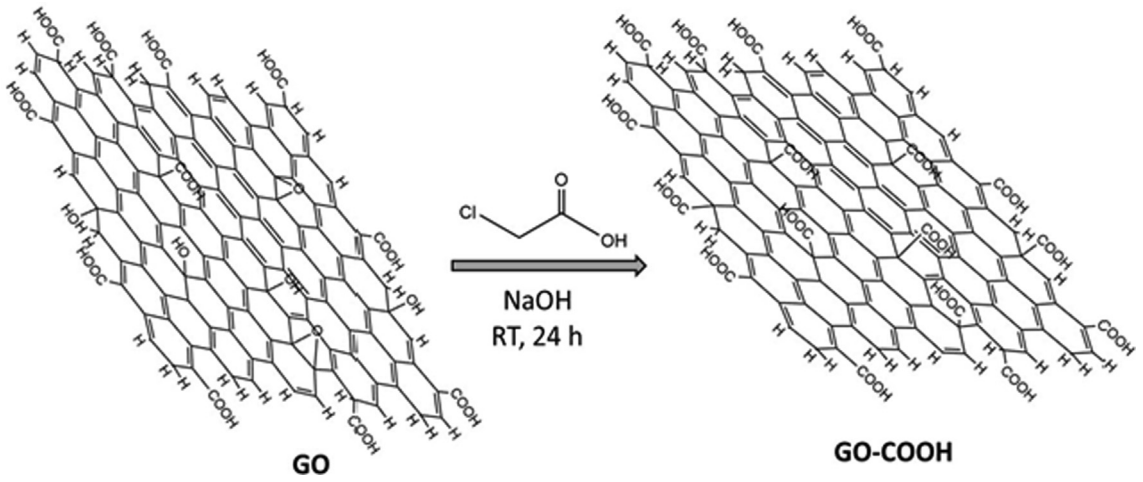

Scheme 3. Scheme of the GO-COOH synthesis.

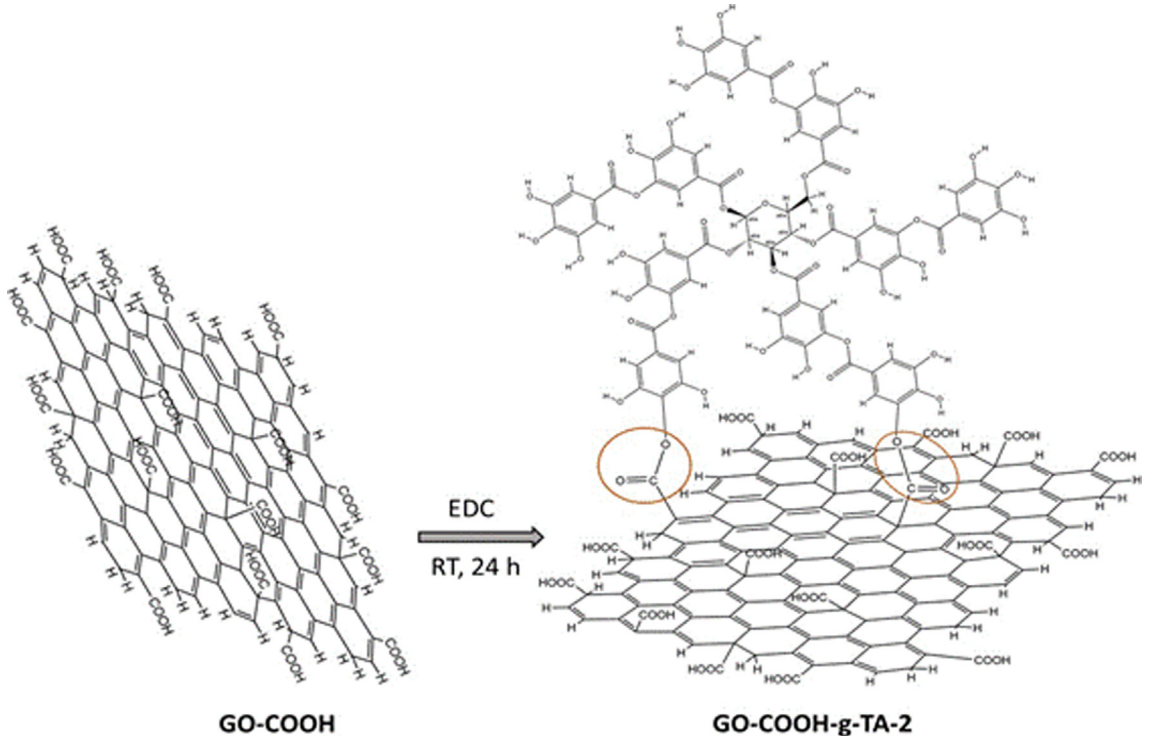

Scheme 4. Schematic representation of the synthesis of GO-COOH-g-TA-2.

layers rich in wrinkles and folded regions, in agreement with observations reported earlier [34]. The fast deoxygenation reaction during exfoliation separates the graphitic sheets, yielding a fuzzy and soapy appearance. Samples obtained via the GO-COOH derivative (Fig. 1c and e) show the thinnest layers, in agreement with results reported in previous works [35,36]. Thus, due to the strong basic conditions in the carboxylation process, most of the remaining carboxylic acid groups will be dissociated, which would provoke a repulsion between the nanosheets, hence resulting in better exfoliated and thinner flakes (in the range of 40–10 nm). In particular, the GO-COOH-g-TA-2 (Fig. 1e) displays a loosely-packed multilayered structure with the largest interlayer spacing and the highest degree of bending, with many foldings at the flake edges. This suggests that a large amount of TA molecules, with the role of dispersant and stabilizer, were grafted onto the GO surface: the repulsive electrostatic interactions between neighboring TA-wrapped sheets make GO layers stable versus re-aggregation, hence GO nanosheets uniformly dispersed were obtained. Conversely, the GO-CO-Cl-g-TA (Fig. 1f) partly preserves the morphology of pristine GO, with staked flakes showing a wide range of thicknesses (30–65 nm), thereby suggesting a lower degree of grafting. It resembles a 3D porous network of wrinkled GO nanosheets.

3.2. Hydrophilicity degree

Water contact angle (CA) study was carried out to assess the change in the hydrophilicity of the nanomaterial upon functionalization. Fig. 2 displays CA values for GO (a), GO-TA, (b) GO-g-TA, (c) and GO-COOH-g-TA-2 (d), and the values for all the samples are

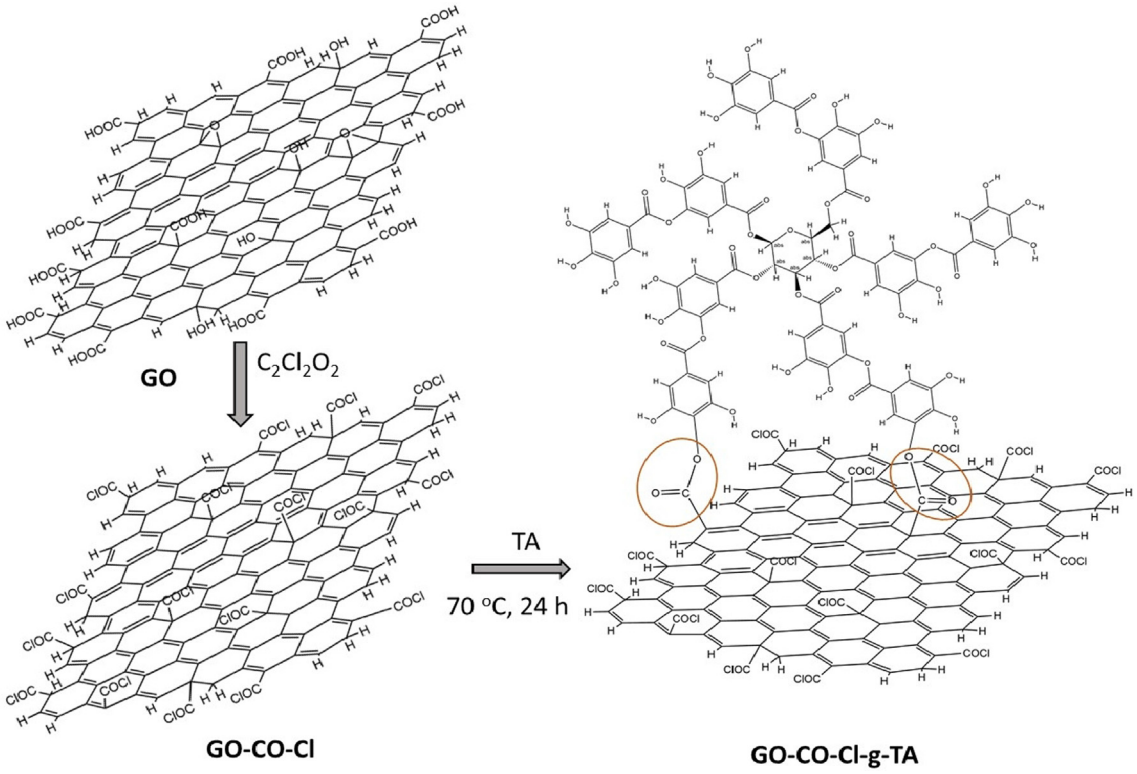

Scheme 5. Illustration of the synthesis of GO-CO-Cl-g-TA.

displayed in Table 1. Pristine GO is hydrophilic (CA ~ 40°) owed to its numerous oxygenated surface groups that enable prompt sample swelling by water absorption. A slight decrease in CA (improved water wettability) is found for the non-covalently functionalized sample, ascribed to the high hydrophilicity of TA [37]. However, for all the covalently-functionalized samples, CA increased, which could be related to the reduction in the amount of carboxylic acids due to the esterification process and the stronger crosslinking among GO sheets, which decreases swelling ability [38]. This is also in agreement with the formation of a partly reduced GO in GO-g-TA, since rGO samples have been reported to be hydrophobic (CA > 90°) [39]. GO-COOH-g-TA-2 shows the highest CA value (~77°), hinting again that it has the highest degree of functionalization, though is still hydrophilic (CA < 90°). It should be noted that the best CA for adsorption of biomolecules and cellular linkage are believe to be between 40° and 75° [40], which suggests that the modified GO samples developed herein would be suitable for biomedical applications. In particular, GO-g-TA (CA ~ 53°) shows great potential for tissue engineering, since the best CA value for attaching cells to implants has been reported to be 55° [41].

3.3. Solubility tests

The solubility and dispersion stability of the functionalized GO samples in different solvents is critical with a view to use them in practical applications. Therefore, their solubility/dispersibility was tested in aqueous media and organic solvents of diverse nature and polarity, in order to compare with the behavior of pristine GO, and the qualitative results obtained are displayed in Table 1. Typical photographs of pristine GO and GO-COOH-g-TA-2 dispersions in water, toluene, NMP, n-hexane, DMF and ethylene glycol after one week preparation are shown in Fig. 3.

Parent GO is fully soluble in NMP, and quite well soluble in water, DMF and propanol, which is consistent with observations reported earlier [42]. Thus, the solubility of GO in water is conditioned by its number of oxygenated groups. Nevertheless, despite its high oxygen content (~32%), it is just somewhat soluble in ethylene glycol, ethanol or methanol, which are protic polar solvents. Such behavior is difficult to be rationalized from the viewpoint of the rule of thumb "like dissolves like": GO contains abundant alcohol moieties on both sides of the rings, and it would be expected to be fully soluble in alcohols. Besides, it was slightly soluble in highly polar aprotic solvents like DMSO. This suggests that besides the solvent polarity, the solubility is influence by factors including the solvent surface tension, dipole moment and Hansen solubility parameters [43]. Accordingly, solvents with high dipole moment values (3.76, 1.67 and 1.85 for NMP, propanol and water) and a surface tension close to the reported surface energy of GO (~60 mN/m [44]) seem to be optimal. Besides, the solubility/dispersibility of GO and the durability of the corresponding solutions are influenced by the chemical configuration of the GO/solvent interface and the interactions between the solvent and the functional groups of GO via H-bonding, which have been reported to decrease in the sequence: water > methanol > ethanol [43]. On the other hand, GO showed poor solubility in nonpolar solvents such as aliphatic CH_3Cl or aromatic toluene though good dispersibility, whereas was completely insoluble in alkanes like pentane or hexane.

Regarding the non-covalently functionalized sample, it was found to be completely soluble in water, DMF, NMP, methanol, ethanol, propanol and ethylene glycol, which is in agreement with its higher degree of hydrophilicity. Thus, previous studies corroborated the solubility of TA in the aforementioned solvents [20]. The numerous phenolic groups of TA are expected to interact strongly with water and alcohols via H-bonding, resulting in improved solubility. Besides, it showed better solubility than pristine GO in

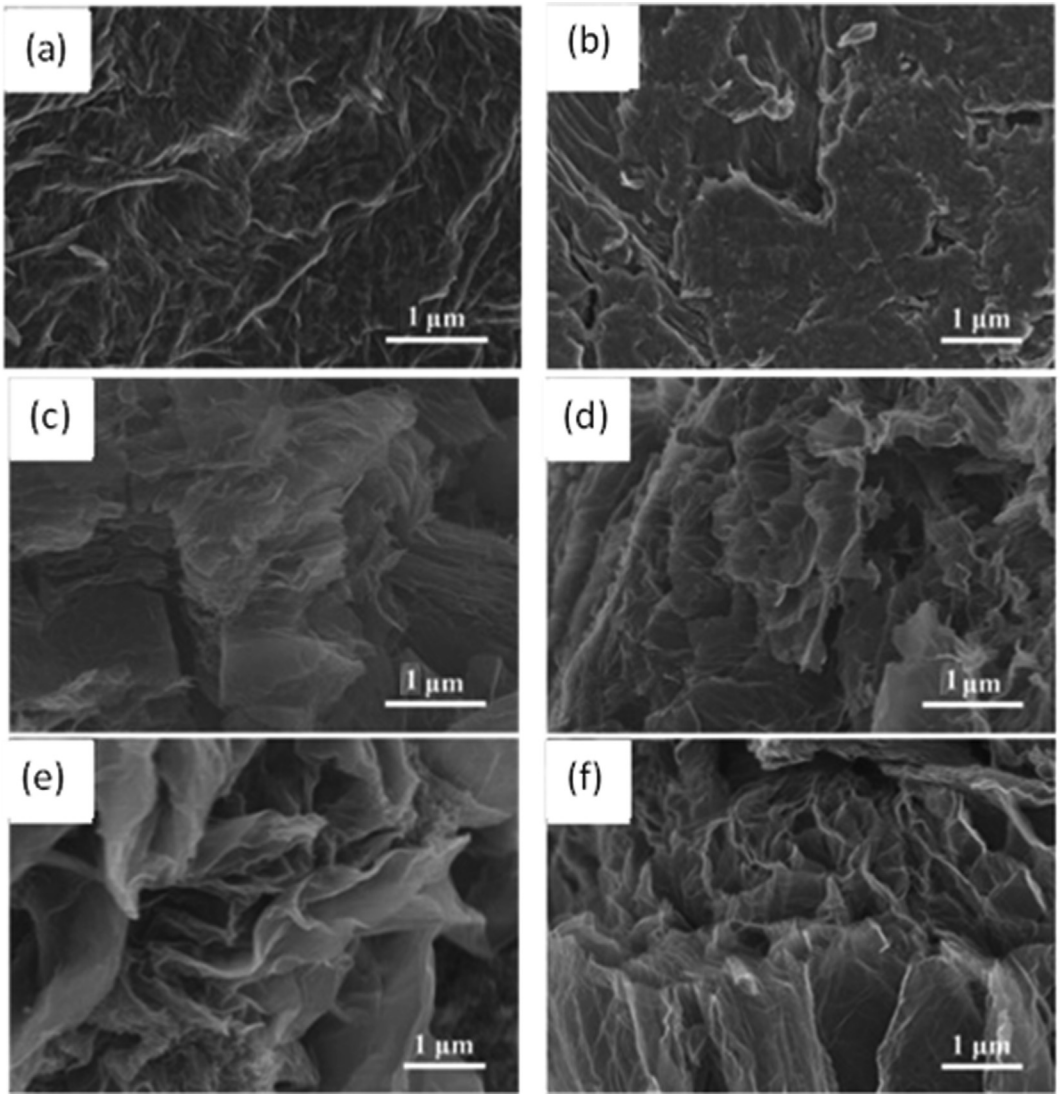

Fig. 1. Representative SEM images of (a) GO, (b) GO-TA, (c) GO-COOH-g-TA-1, (d) GO-g-TA, (e) GO-COOH-g-TA-2, (f) GO-CO-Cl-g-TA.

polar aprotic solvents like DMSO. Conversely, it was insoluble in nonpolar solvents like $CHCl_3$. On the other hand, the covalently functionalized samples were partially/slightly soluble in aqueous solution and polar protic solvents, and the solubility decreased upon increasing degree of grafting (Table 1). Thus, GO-COOH-g-TA-2 was almost insoluble in DMF and NMP (Fig. 3). They also showed reduced dispersibility in DMSO. However, due to their more hydrophobic nature, they were more easily dispersed in low polar or nonpolar solvents like toluene or THF, respectively (Fig. 3d). The reduction of hydrogen bonds triggered by the covalent grafting of TA molecules renders the nanomaterial surface more hydrophobic, as discussed earlier, thus enabling improved dispersion in organic solvents.

3.4. FT-IR study

FTIR measurements were carried out to corroborate the functionalization processes and get insight about the amount of functional groups in the different samples, and the spectra are compared in Fig. 4**.** A zoom of the spectra showing the features in the fingerprint region is shown in Figure S3. The spectrum of pristine GO has a wide feature arising from the O-H stretch of hydroxyls and carboxylic acids at 3480 cm^{-1}. The sp^3 C–H stretching bands (due to defects) are found at 2930 and 2850 cm^{-1}, the benzene ring C–C stretch at 1625 cm^{-1}. Besides, a strong C = O stretching is detected at ~ 1730 cm^{-1}, arising from the carboxylic acids, and the O–H deformation takes place at ~ 1390 cm^{-1} [45]. Other peaks at about 1280 and 1040 cm^{-1} arise from the C-O stretching of epoxides [13]. The spectrum of GO-COOOH (Figure S4) shows a broader peak within 2800–3600 cm^{-1} compared to pristine GO, since most of the hydroxyl and epoxy groups have been transformed into carboxylic acid moieties during the oxidation process. This is further corroborated by the almost disappearance of the peaks arising from the epoxides and the strong increase in the intensity of the C = O stretching from the carboxylic acids.

Regarding the spectrum of raw TA, a very broad O-H stretching is found within 3000–3700 cm^{-1} from H-bonded phenol and carboxylic acid groups [46]. The C = O and C-O stretching of quinic acid esters appear at 1718 and 1220 cm^{-1}, respectively. Moreover, features ranging between 1600 and 1400 cm^{-1} correspond to aromatic units. Regarding the non-covalently functionalized GO-TA sample, a widening and downshift of the O-H stretching is found in comparison with the parent GO. Similarly, a change in the C = O stretching to lower frequencies is observed, which reveals the existence of strong H-bonds with the OH moieties of TA. Analogous behavior has been described for GO non-covalently func-

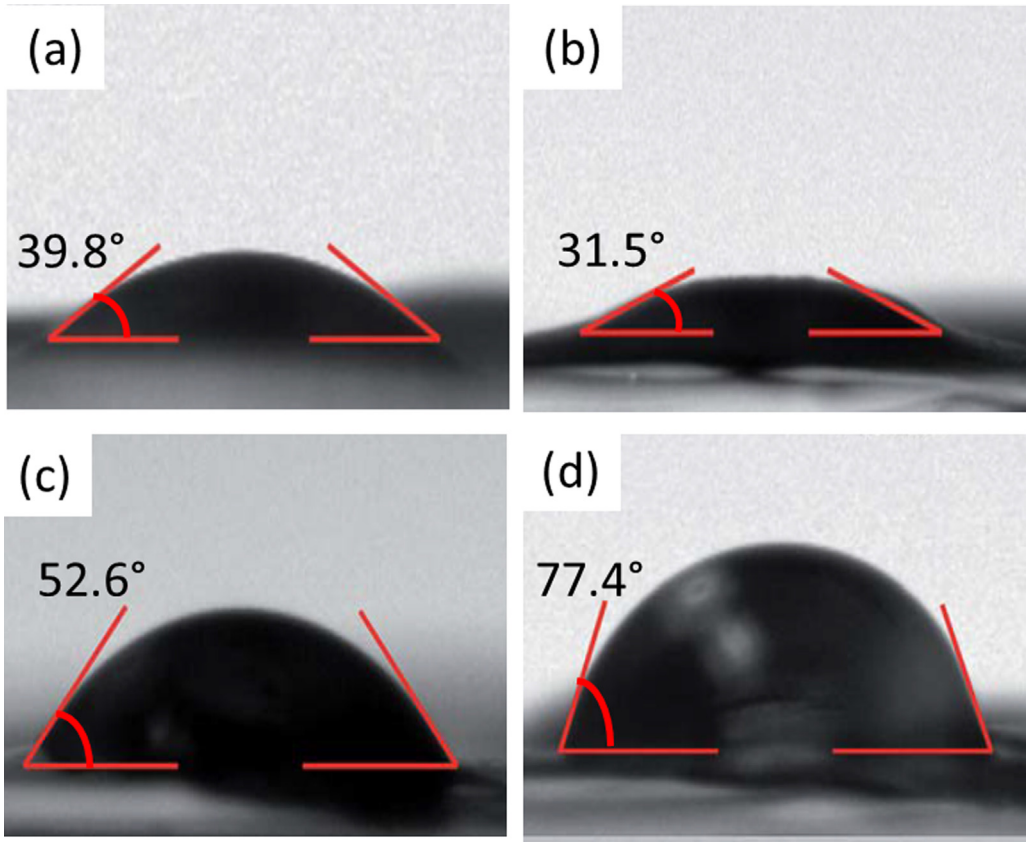

Fig. 2. CA values for (a) GO, (b) GO-TA, (c) GO-g-TA, (d) GO-COOH-g-TA-2.

Table 1
Water contact angle (CA) and solubility of GO and the functionalized samples in the indicated solvents.

Nanomaterial	CA (°)	Water	NMP	DMSO	DMF	Toluene	CH_3Cl	THF
GO	39.8	FS/PS	FS	PS/SS	S/PS	IS	SS	IS
GO-TA	31.5	FS	FS	PS	FS	IS	IS	IS
GO-g-TA	52.6	PS	FS	PS	PS	SS	SS	SS
GO-COOH-g-TA-1	69.3	PS	PS	SS	PS	SS	PS	PS
GO-COOH-g-TA-2	77.4	PS	IS	IS	SS/IS	PS	PS	PS
GO-CO-Cl-g-TA	49.8	FS/PS	FS	PS	PS/SS	SS	SS	SS/IS
Nanomaterial		**Propanol**	**Methanol**	**Ethanol**	**Pentane**	**Hexane**	**Acetone**	**EG**
GO		SS/PS	SS	PS	IS	IS	IS	PS
GO-TA		FS	FS	FS	IS	IS	IS	FS
GO-g-TA		PS	SS/PS	SS/PS	IS	IS/SS	IS	PS
GO-COOH-g-TA-1		PS	PS	PS	SS	SS	IS	SS
GO-COOH-g-TA-2		SS/PS	PS	PS	PS	SS	IS	PS
GO-CO-Cl-g-TA		FS/PS	SS	SS	IS	IS	IS	PS

IS: Insoluble; SS: Slightly soluble; PS: Partially soluble.; FS: Fully soluble.; EG: ethylene glycol.

tionalized with other biomolecules like proteins and biopolymers such as polyethylene glycol PEG [7,47].

The spectra of GO-COOH-g-TA-1 and GO-COOH-g-TA-2 (Fig. 4) show a broad peak within 2800–3600 cm^{-1}, similar to that found in GO-COOH, albeit with reduced intensity, since part of the carboxylic acids are covalently bonded to catechol moieties of TA. The drop is stronger for GO-COOH-g-TA-2, corroborating that the esterification is more effective using EDC activation. On the other hand, a new peak related to the C = O stretching of aromatic esters appears close to 1765 cm^{-1}. Thus, the C = O stretching of esters typically appears in the range of 1703–1750 cm^{-1}, but this frequency is increased in the presence of electron-withdrawing substituents like phenyls, since they decrease the electrophilicity of the carbonyl carbon [48] and reduce the number of resonance forms that stabilize the molecule [49]. An upshift in the C = O frequency has been observed in phenyl esters of benzoic acid, in which the benzyl part lied in a different plane from the carboxyl group [50]. Therefore, the appearance of this new peak corroborates the esterification reaction and suggests that aromatic rings of GO and TA are not coplanar. Besides, the peak is considerably stronger for GO-COOH-g-TA-2, indicative of a higher degree of grafting.

Regarding GO-g-TA, prepared via direct esterification reaction of GO with TA, the peak at about 1765 cm^{-1} is also observed, albeit with lower intensity, indicating lower degree of grafting, as could be expected. Nonetheless, a very intense band related to the C-O stretching of ethers is found at about 1100 cm^{-1} which is not observed in the other samples nor in pristine GO [45]. This indi-

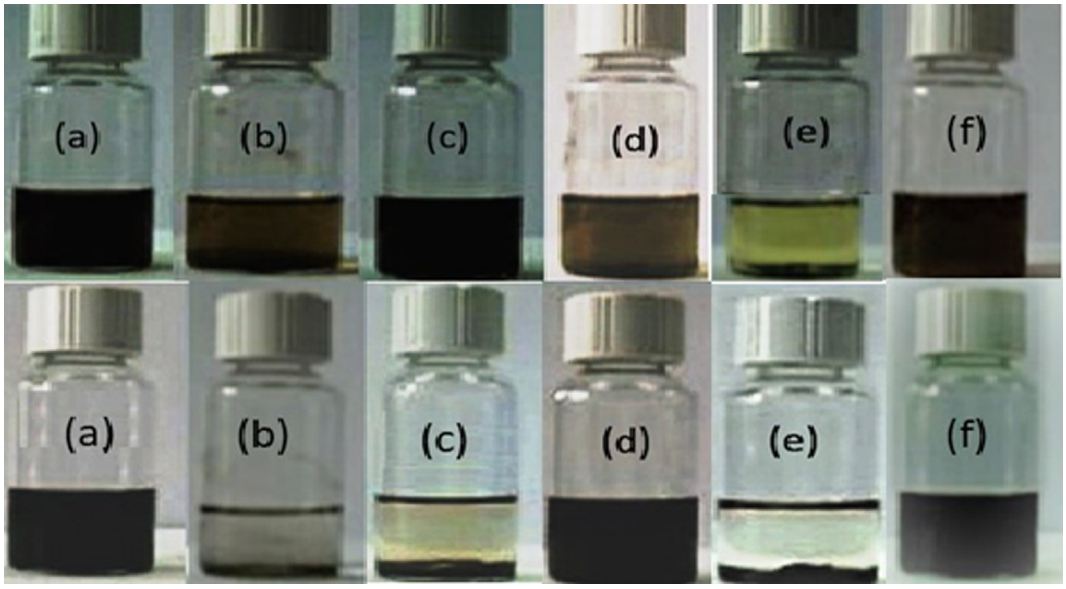

Fig. 3. Photographs of the GO dispersions (top) and GO-COOH-g-TA-2 (bottom) after a week in the following solvents: (a) Water; (b) *N,N*-dimethylformamide; (c) N-methyl-2-pyrrolidone; (d) toluene; (e) n-hexane; (f) ethylene glycol.

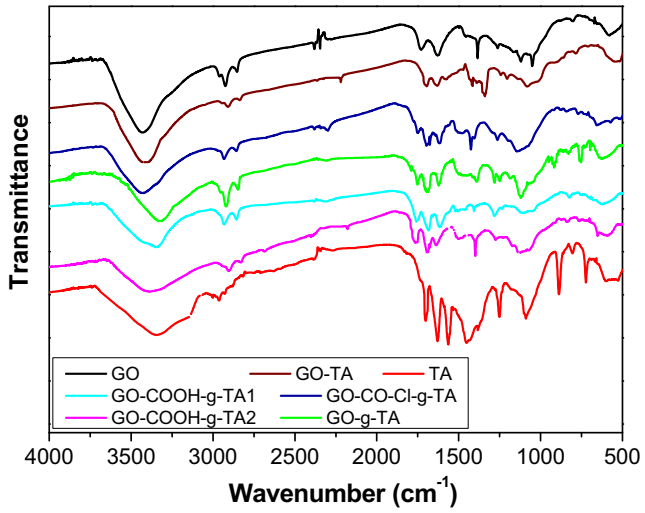

Fig. 4. MIR spectra of neat GO, TA, and the non-covalently and covalently functionalized samples synthesized in this work.

cates that the grafting in this sample also takes place via ring opening of the epoxy moieties, which is further corroborated by the disappearance of the band related to epoxy C-O stretching around 1040 cm^{-1}. Besides, the strength of the sp^3 C–H stretching bands rises significantly, since the ring opening yields extra methylene groups, yet another confirmation of the grafting via epoxy moieties [51]. Conversely, the O-H stretching shows lower intensity and is noticeably changed towards lower wavenumber compared to that of GO, indicating that not only covalent grafting but also H-bonding interactions play a key role in this sample. Similar behavior of diminution in intensity of the OH stretching band was found when other natural reducing agents like vinegar or lemon juice [52] were used for the green synthesis of rGO from GO.

Focusing on GO-CO-Cl-g-TA, prepared via acylation with oxalyl chloride, also shows the peak at about 1765 cm^{-1}, albeit less intense than in the other samples, suggesting lower grafting degree. To get insight about the degree of esterification, the ratio between the height of this peak and a reference band (the C-C stretching of benzene rings, unchanging) at 1625 cm^{-1} was calculated. The values obtained were 0.65, 0.67, 0.78, 0.98 for GO-CO-Cl-g-TA, GO-g-TA, GO-COOH-g-TA-1 and GO-COOH-g-TA-2, respectively. It should be noted that though these data cannot be used to quantify the esterification degree, they indicate the samples with higher extent of grafting. Besides, the trend in the grafting degree attained is in good agreement with that obtained from TGA analysis, as discussed later. It is also worthy to note that the O-H stretching in GO-CO-Cl-g-TA shows reduced intensity, as found in the other samples, and the band is significantly broadened, also indicative of H-bonding interactions. Besides, an additional band due to the C-Cl stretch emerges at 700 cm^{-1} [45]. Overall, FT-IR analysis corroborates the success of the functionalization processes carried out in this work.

3.5. Raman study

To get more evidence on the strength of the GO-TA interactions, Raman spectra were acquired, and the comparison for the different samples is provided in Fig. 5. The main characteristics found in graphitic nanomaterials can be observed: the so-called G band around 1595 cm^{-1}, common to all sp^2 nanocarbons, ascribed to the in-plane vibration of C-C bonds, and a D band at 1345 cm^{-1} associated with defects and deviations from perfect order in the sp^2 graphite lattice [53]. Regarding TA, the C = C and C = O stretching of benzene units appear as sharp bands at 1700 cm^{-1} and 1580 cm^{-1}, respectively [54], and the C–O stretching and O–H bending of phenol moieties are found at 1130 cm^{-1} and 1325 cm^{-1}, respectively. Peaks around 1130 and 1700 cm^{-1} are also observed in the non-covalently functionalized sample, albeit shifted to higher wavenumber, indicative of a change in the C-O bond length, likely due to interactions (polar and hydrogen bonding) with oxygenated moieties of GO. Shifts in TA bands have been previously reported due to interactions with proteins and DNA [55]. Conversely, the D and G band are shifted in GO-TA towards lower wavenumber, appearing at an intermediate position between those of pristine GO and those of TA, which is reasonable for a mixture with non-covalent interactions between the components.

On the other hand, the covalently functionalized samples only show the characteristic peaks of graphene materials albeit shifted

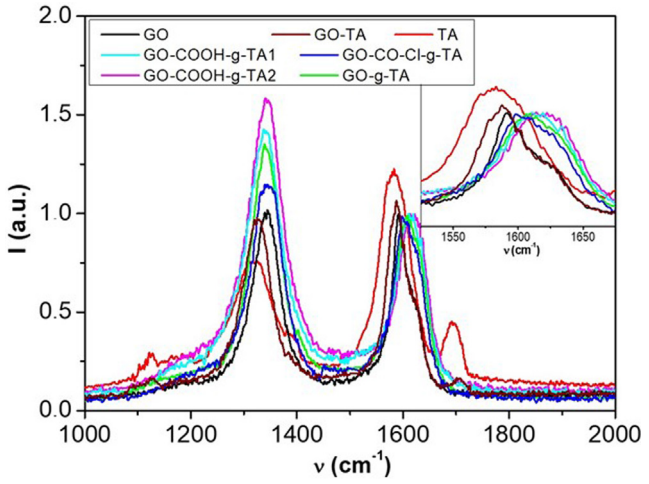

Fig. 5. Comparison of the Raman spectrum of neat GO, TA, and the non-covalently and covalently functionalized samples synthesized in this work. The inset is a magnification of the region between 1530 and 1680 cm^{-1} to show the changes in the wavenumber of the G band.

to higher wavenumber. This upshift of the G band is likely an outcome of the incorporation in the graphene structure of electron-donor groups [53]. Polyphenolic compounds like TA can act as an electron-donor groups [56], consequently triggering a change in the G band position. Besides, the frequency of this band is influenced by the number of graphene layers: as the number of layers increases, the band position shifts to a higher frequency. Accordingly, the upshift of the G band could also be indicative of a transition from few layers to multilayer GO [57]. In fact, TA could also act as a crosslinker between the GO sheets, thus leading to a multilayered structure. This is consistent with SEM observations, which revealed a multilayered structure for GO-COOH-g-TA-2, with the largest interlayer spacing. Furthermore, this upshift can be attributed to an increase in the number of defects in the graphitic layers. Indeed, the upshift is more pronounced upon increasing grafting degree, as it is clear from the inset of Fig. 5, being about 55 cm^{-1} for GO-COOH-g-TA-2, thus corroborating its higher degree of grafting, as already inferred from the IR spectrum. Conversely, for GO-CO-Cl-g-TA, the upshift is only $\sim$ 10 cm^{-1}, suggesting weaker GO-TA interactions. Therefore, the results obtained from the Raman spectra are in very good agreement with those derived from IR spectroscopy.

The strength of the D band is directly dependent on the defect concentration of the graphene layers and depends on the defect type (ie. vacancies, interstitial impurities, sp^3 hybridation [58]). The I_D/I_G ratio is a quantity that enables to estimate the defects in graphenic nanomaterials: the higher this ratio, the higher the number of defects [53]. The I_D/I_G values calculated herein are gathered in Table 2. Pristine GO and GO-TA show an I_D/I_G ratio close to 1, which is in agreement with results stated earlier for GOs with moderate oxygen content [59]. Conversely, the covalently functionalized samples show higher values, the maximum being 1.62 for GO-COOH-g-TA-2. Thus, a steady rise in this ratio is found with increasing grafting degree, which corroborates a drop in the structural order due to the increase in the number of atoms with sp^3 hybridization. Taking into account the terminology introduced by Ferrari *et al.* [60] for the interpretation of the Raman spectra of graphene, the I_D/I_G ratio follows a two-stage growth: Stage 1 corresponds to low-defect graphene, while stage 2 corresponds to disordered graphene. In stage 1, the intensity of the D band is proportional to the defect concentration. However, in stage 2, the effect of the electron lifetime predominates, and the relationship becomes more complicated. The range of values obtained herein for the covalently modified samples are lower than 3.5, hence likely correspond to stage 1 (low defect degrees), in which transition from sp^2 to sp^3 C atoms predominates [58]. A similar trend of increase in the I_D/I_G ratio has been reported upon grafting of graphene to molecules such as pentamethyldiethylenetriamine [61] or polymers like polymethyl methacrylate (PMMA) [62].

The increased I_D/I_G values revealed by Raman spectroscopy relative to the starting GO demonstrate the success of the grafting processes developed herein.

3.6. Thermogravimetric analysis

To assess the heat resistance of the functionalized samples, TGA was carried out under an inert environment, and the thermograms recorded for the different samples are compared in Fig. 6. Besides, Table 2 summarizes the characteristic temperatures of degradation: onset (T_i), 10 wt% mass loss (T_{10}) and peak (T_{max}, maximum of the first derivative DTG). The pristine GO displays a one-stage decomposition with a Ti close to 125 °C and a Tmax of 235 °C, showing around 38% weight loss before 250 °C. This main step likely corresponds to the removal of epoxide, hydroxyl and carboxylic acids [13], as inferred from the IR analysis. Moreover, a minor steady loss can be detected above 250 °C, due to further removal of oxygenated moieties. Similar thermogram was found for GO-COOH intermediate (**Figure S5**), albeit slightly shifted to lower temperatures, showing about 43% weight loss below 250 °C. On the other hand, TA starts to decompose at about 190 °C and shows a major mass loss before 360 °C, attributed to the removal of CO_2 and benzenetriol from the outer layer of gallic acid units, as reported previously [63]. At higher temperature, the char produced is mostly from the crosslinking of the inner gallic acid units, leading to a remaining residue of about 25%.

The thermogram of the non-covalently functionalized sample is analogous to the described for GO though slightly shifted to higher values, likely due to the strong H-bonding interactions with TA that result in a denser packing and higher thermal stability. Thus,

Table 2
I_D/I_G ratio, characteristic temperatures of degradation obtained from TGA analysis: onset (T_i), 10% mass loss (T_{10}), peak (maximum of the 1st derivative) T_{max}, estimated grafting degree (GD) and percentage of bacterial inhibition (BI%).

Sample	I_D/I_G	T_i (°C)	T_{10} (°C)	T_{maxI} (°C)	T_{maxII} (°C)	GD (%)	$BI_{E.coli}$ (%)	$BI_{S.aureus}$ (%)
GO	1.02	124.6	180.2	235.1	–	–	40.8	59.6
TA		188.5	261.4	322.5	–	–	18.6	21.5
GO + TA*	–	–	–	–	–	–	56.8	70.7
GO-TA	0.94	146.2	200.1	247.2	–	–	61.4	74.6
GO-g-TA	1.35	165.1	247.7	298.7	360.1	–	82.6	90.5
GO-COOH-g-TA-1	1.44	169.4	245.8	288.6	366.5	34.4	99.3	99.9
GO-COOH-g-TA-2	1.62	174.2	249.7	303.2	371.5	38.9	99.9	99.9
GO-CO-Cl-g-TA	1.14	146.2	205.6	254.3	358.6	25.1	79.7	85.3

*Reference sample prepared by direct addition of GO and TA to the solution.

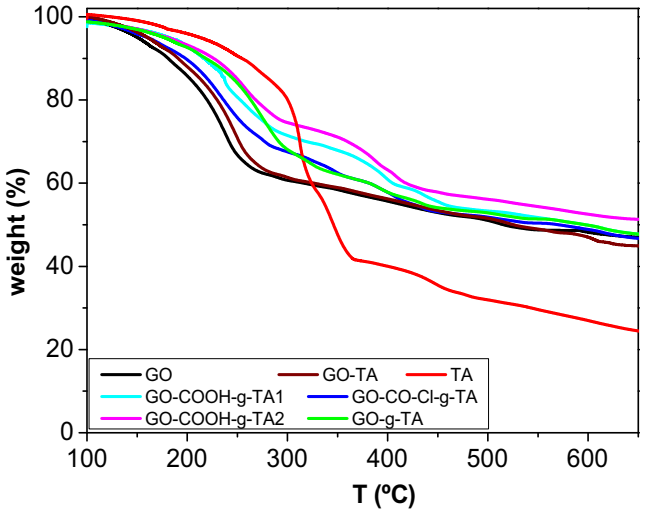

Fig. 6. TGA thermograms of GO, TA and the non-covalently and covalently functionalized samples.

T_i and T_{max} increased by about 22 °C compared to pristine GO. Similar behaviour of stability enhancement has been reported for TA complexes with lignocellulose [64] and chitin nanoparticles [65], attributed to extensive H-bonding. In fact, this type of interaction has been reported as a key strategy to improve thermal stability in biological molecules such as proteins [66].

The covalently functionalized nanomaterials exhibit two most important decomposition stages. The lower temperature one is equivalent to that described above for raw GO and GO-COOH, and likely arises from the elimination of the remaining functional groups. The mass loss of this stage drops progressively with increasing grafting degree, corroborating a diminution in the amount of surface groups. This can be explained considering that the higher the number of carboxylic acid groups of GO-COOH that have reacted with the OH groups of TA, the fewer the number of residual oxygenated moieties on the GO surface that would decompose during this step. Hence, the grafting degree (GD) [51] was roughly estimated from weight loss of this stage as relative difference between the percentage of surface functional groups of GO-COOH (Figure S5) and that of the grafted samples, and the values obtained are collected in Table 2. Accordingly, GO-COOH-g-TA-2 shows the highest degree of covalent bonding followed by GO-COOH-g-TA-1, while GO-CO-Cl-g-TA has the lowest, consistent with the trend found from the FT-IR spectra (Fig. 1). It should be noted that it is not feasible to calculate the grafting degree of GO-g-TA from TGA analysis since in this sample the grafting process takes place also via epoxy groups, and these could have been reduced in the presence of TA. The synthesis of the acid-functionalized GO followed by activation of the carboxylic acids with EDC seems to be the most effective grafting approaching, being superior to the direct esterification reaction or the formation of the acyl chloride-derivative in terms of selectivity and the yield of attached functional groups. Besides, EDC and its urea byproduct are soluble in aqueous solution and can be easily eliminated from the reaction medium [67], leading to a greener esterification process.

Regarding the characteristic degradation temperatures, a progressive rise is found as the degree of grafting rises (Table 2), which likely arises from the stronger linkage between the layers, as described earlier in crosslinked GO/chitosan nanocomposites [63]. The increase in crosslinking density makes molecular mobility difficult, hence reduces the amount of sample decomposed during the first step. Thus, T_i and T_{10} increased by>40 and 60 °C, respectively, for GO-g-TA, GO-COOH-g-TA-1 and GO-COOH-g-TA-2, compared to pristine GO. **S**ince TA has numerous OH groups, it can behave as a crosslinker for the GO sheets, as mentioned earlier, leading to the formation of a supramolecular arrangement which would prevent the flow out of the decomposed fragments, and this is reflected in higher decomposition temperatures. Also, it was found that the thermal interfacial resistance GO-biopolymer decreases with the formation of chemical bonds [68]. Besides, the complex condensed aromatic structure of TA can delay the decomposition reactions. Thus, TA has been found to be an effective flame retardant of different polymers such as polylactide acid (PLA) [69]. Analogous phenomenon of improvement in thermal stability has been described earlier upon grafting TA to other polymers like polyurethane [70] or biopolymers such as cotton, wool, or silk [71]. Overall, TGA measurements corroborate the improved thermal stability for the grafted samples, which is of great interest from an application viewpoint in sensors or electronic devices.

3.7. Antibacterial activity

With the view to use the synthesized samples in the biomedical arena, it is interesting to evaluate their antibacterial activity. Thus, the percentage of microbial inhibition against Gram-positive *S. aureus* and Gram-negative *E. coli* is collected in Table 2. For the sake of comparison, the percentages of bacterial inhibition of neat GO, TA and a reference sample (GO + TA) prepared by direct addition of GO and TA to the solution are also included in the Table.

Pristine GO shows significant antibacterial activity versus both bacteria, in agreement with results reported previously [7,72]. Though the bactericide action of graphene and its derivatives it is not fully clear yet, several mechanisms have been suggested [73,74]. In particular, impairment of the bacteria membrane produced by direct interaction between the sharp edges of GO layers and the bacteria walls, microorganism confining within the GO layers and reactive oxygen species (ROS) formation [73,74] can account for the observed decrease in bacterial growth. Thus, GO sheets can yield radicals that react with the C = O moieties of amide bonds in the wall of the microorganism and impair the cellular constituents including proteins, DNA, lipids, etc., hence rescinding the microorganism. Consequently, the Gram-negative comprising an outer thin layer of peptidoglycan become more resilient to the membrane impairment than the Gram-positive missing the outside membrane, in agreement with the results obtained herein.

Both non-covalently and covalently functionalized samples show higher antibacterial activity that neat GO against both bacteria. In all the samples, the bactericide effect is systematically stronger against *S. aureus*. Also, the covalently functionalized samples show higher biocide action, which rises gradually upon increasing grafting degree. These data corroborate that the presence of TA notably improves the antibacterial activity of GO against both types of bacteria, which can be explained considering the exceptional antibacterial properties of this polyphenolic compound. Thus, GO layers in the synthesized samples are covered by TA, which has been reported to pass through the microorganism wall to the interior membrane and bind to bacteria proteins via hydrophobic interactions and hydrogen bonds [75], thus inhibiting the bacteria metabolism. Furthermore, TA hinders amino acid and sugar ingestion, which restricts bacterial growth. Additionally, TA behaves as a blocker of the NorA efflux pump, the first-line of defense for bacteria against antimicrobials, and this is regarded the key mechanism accounting for its antibacterial activity [76]. In fact, preceding works [77] have shown the strong antibacterial activity of TA versus both bacteria tested, which increased progressively upon increasing concentration of phenolic hydroxyl groups. Also, Gram-positive microbes were found to have additional vulnerability to TA than Gram-negative ones, which is consistent with

the results obtained in this work. In our study, it appears to be a synergistic effect of both TA and GO on bacteria killing, since all the grafted samples present significantly higher inhibition values than the reference sample (GO + TA). In particular, a very effective bactericide effect, up to 99.9%, is found for GO-COOH-g-TA-1 and GO-COOH-g-TA-2 against *S. aureus*. Thus, these samples with high grafting degree have great potential to regulate the growth of human pathogenic bacteria, thus preventing the spread of human diseases.

4. Conclusions

Different GO samples covalently and non-covalently functionalized with TA have been successfully obtained via easy, inexpensive and ecofriendly processes. Four different esterification approaches (direct, via acid-functionalized GO, via carbodiimide activation and via acylation with oxalyl chloride) have been tested. Microscopic observations revealed that TA molecules acted as both dispersant and stabilizer agents of the nanomaterial, resulting in uniformly exfoliated nanosheets. Infrared and Raman spectra supported the accomplishment of the grafting reactions, revealing the appearance of signals associated with the ester groups. The grafting of TA onto GO surface led to improved solubility/dispersibility in organic solvents, higher thermal resistance and better antibacterial activity. The activation of the carboxylic acid groups with carbodiimide resulted in the highest degree of grafting, as inferred from IR spectra and TGA measurements. Besides, this sample showed exceptional increments in the characteristic degradation temperatures (by up to 60 °C) compared to pristine GO. Further, a synergistic effect of both GO and TA on inhibiting bacterial growth was found, which increased gradually upon increasing degree of grafting, and was found to be systematically stronger on Gram-positive bacteria. This study paves the way towards the synthesis of green graphene derivatives to be applied in the biomedical field, as sensor devices or for the development of ecological nanocomposites.

Author contributions

C.S.-U. experimentation; M.P.S. and S.V-L. review editing; A.M. D.-P. conceptualization, original draft preparation, supervision.

Statements and declarations

The authors declare that there is no conflict of interest.

Funding

Financial support from Ministerio de Ciencia, Innovacion y Universidades (MICIU) via grant number PGC2018-093375-B-I00 is gratefully acknowledged. Funding from the Community of Madrid within the framework of the Multiyear Agreement with the University of Alcalá for "Stimulus to Excellence for Permanent University Professors", Ref. EPU-INV/2020/012 is also acknowledged

Data availability statement

The data presented in this study are available on request from the corresponding author.

Declaration of Competing Interest

The authors declare that they have no known competing financial interests or personal relationships that could have appeared to influence the work reported in this paper.

Appendix A. Supplementary data

Supplementary data to this article can be found online at https://doi.org/10.1016/j.molliq.2022.119104.

References

[1] K.S. Novoselov, A.K. Geim, S.V. Morozov, D. Jiang, Y. Zhang, S.V. Dubonos, I.V. Grigorieva, A.A. Firsov, Electric field effect in atomically thin carbon films, Science 306 (5696) (2004) 666–669.
[2] P. Zare, M. Aleemardani, A. Seifalian, Z. Bagher, A.M. Seifalian, Graphene Oxide: Opportunities and Challenges in Biomedicine, Nanomaterials 11 (5) (2021) 1083.
[3] A.M. Díez-Pascual, M.A. Gómez-Fatou, F. Ania, A. Flores, Nanoindentation in polymer nanocomposites, Prog. Mater. Sci. 67 (2015) 1–94.
[4] D. Chen, H. Feng, J. Li, Graphene Oxide: Preparation, Functionalization, and Electrochemical Applications, Chem. Rev. 112 (11) (2012) 6027–6053.
[5] J.A. Luceño-Sánchez, A.M. Díez-Pascual, Grafting of Polypyrrole-3-carboxylic Acid to the Surface of Hexamethylene Diisocyanate-Functionalized Graphene Oxide, Nanomaterials 9 (2019) 1095.
[6] O.C. Compton, S.T. Nguyen, Graphene Oxide, Highly Reduced Graphene Oxide, and Graphene: Versatile Building Blocks for Carbon-Based Materials, Small 6 (6) (2010) 711–723.
[7] A.M. Díez-Pascual, A.L. Diez-Vicente, Poly(propylene fumarate)/Polyethylene Glycol-Modified Graphene Oxide Nanocomposites for Tissue Engineering, ACS Appl. Mater. Interfaces 8 (28) (2016) 17902–17914.
[8] V. Georgakilas, M. Otyepka, A.B. Bourlinos, V. Chandra, N. Kim, K.C. Kemp, P. Hobza, R. Zboril, K.S. Kim, Functionalization of Graphene: Covalent and Non-Covalent Approaches, Derivatives and Applications. *Chem. Rev*. 112 (11) (2012) 6156–6214.
[9] D. Yu, Y. Yang, M. Durstock, J.B. Baek, L. Dai, Soluble P3HT-Grafted Graphene for Efficient Bilayer-Heterojunction Photovoltaic Devices, ACS Nano 4 (2010) 5633–5640.
[10] Y. Xu, Z. Liu, X. Zhang, Y. Wang, J. Tian, Y. Huang, Y. Ma, X. Zhang, Y. Chen, A Graphene Hybrid Material Covalently Functionalized with Porphyrin: Synthesis and Optical Limiting Property, Adv. Mater. 21 (12) (2009) 1275–1279.
[11] C.E. Hamilton, J.R. Lomeda, Z. Sun, J.M. Tour, A.R. Barron, High-yield organic dispersions of unfunctionalized graphene, Nano Lett. 9 (2009) 3460–3462.
[12] S.B. Bon, L. Valentini, R. Verdejo, J.L.G. Fierro, L. Peponi, M.A. Lopez-Manchado, J.M. Kenny, Plasma Fluorination of Chemically Derived Graphene Sheets and Subsequent Modification With Butylamine, Chem. Mater. 21 (2009) 3433–3438.
[13] J.A. Luceño-Sánchez, G. Maties, C. Gonzalez-Arellano, A.M. Diez-Pascual, Synthesis and Characterization of Graphene Oxide Derivatives via Functionalization Reaction with Hexamethylene Diisocyanate, Nanomaterials 8 (11) (2018) 870.
[14] S. Georgitsopoulou, N.D. Stola, A. Bakandritsos, V. Georgakilas, Advancing the boundaries of the covalent functionalization of graphene oxide, Surfaces and Interfaces 26 (2021) 101320.
[15] J.S. Park, H.-K. Na, D.-H. Min, D.-E. Kim, Desorption of single-stranded nucleic acids from graphene oxide by disruption of hydrogen bonding, Analyst 138 (2013) 1745–1749.
[16] A.M. Pandele, C. Andronescu, E. Vasile, I.C. Radu, P. Stanescu, H. Iovu, Non-covalent functionalization of GO for improved mechanical performances of pectin composite films, Composites Part A: Applied Science and Manufacturing 103 (2017) 188–195.
[17] M. Hassanisaadi, G.H.S. Bonjar, A. Rahdar, S. Pandey, A. Hosseinipour, R. Abdolshahi, Environmentally Safe Biosynthesis of Gold Nanoparticles Using Plant Water Extracts, Nanomaterials 11 (2021) 2033.
[18] C. Sainz-Urruela, S. Vera-López, M.P. San Andrés, A.M. Díez-Pascual, Graphene-Based Sensors for the Detection of Bioactive Compounds: A Review, Int. J. Mol. Sci. 22 (2021) 3316.
[19] J.-C.-Y. Lai, H.-Y. Lai, N.K. Rao, S.-F. Ng, Treatment for diabetic ulcer wounds using a fern tannin optimized hydrogel formulation with antibacterial and antioxidative properties, J. Ethnopharmacol. 189 (2016) 277–289.
[20] L. Ruofei, Z. Xiaoqiang, C. Xinxiu, Z. Yagang, Z. Xingjie, Z. Letao, Medical Applications Based on Supramolecular Self-Assembled Materials From Tannic Acid, Frontiers in Chemistry 8 (2020) 871.
[21] Z. Gao, I. Zharov, Large pore mesoporous silica nanoparticles by templating with a nonsurfactant molecule, tannic acid, Chem. Mater. 26 (2014) 2030–2037.
[22] G. Ghigo, S. Berto, M. Minella, D. Vione, E. Alladio, V.M. Nurchi, J. Lachowicz, P. G. Daniele, New insights into the protogenic and spectroscopic properties of commercial tannic acid: The role of gallic acid impurities, New J. Chem. 42 (2018) 7703–7712.
[23] L. Cao, Z. Li, K. Su, B. Cheng, Hydrophilic Graphene Preparation from Gallic Acid Modified Graphene Oxide in Magnesium Self-Propagating High Temperature Synthesis Process, Sci. Rep. 6 (2016) 35184.
[24] I. Kaminska, M.R. Das, Y. Coffinier, J. Niedziolka-Jonsson, J. Sobczak, P. Woisel, J. Lyskawa, M. Opallo, R. Boukherroub, S. Szunerits, Reduction and Functionalization of Graphene Oxide Sheets Using Biomimetic Dopamine Derivatives in One Step, Acs Applied Materials & Interfaces 4 (2012) 1016.

[25] O. Akhavan, M. Kalaee, Z.S. Alavi, S.M.A. Ghiasi, A. Esfandiar, Increasing the antioxidant activity of green tea polyphenols in the presence of iron for the reduction of graphene oxide, Carbon 50 (2012) 3015–3025.
[26] Z. Bo, X. Shuai, S. Mao, H. Yang, J. Qian, J. Chen, J. Yan, K. Cen, Green preparation of reduced graphene oxide for sensing and energy storage applications, Sci. Rep. 4 (2014) 4684.
[27] Y. Lei, Z. Tang, R. Liao, B. Guo, Hydrolysable tannin as environmentally friendly reducer and stabilizer for graphene oxide, Green Chem. 13 (2011) 1655–1658.
[28] A.V. Singhal, R. George, A.K. Sharma, D. Malwal, I. Lahiri, Development of superhydrophillic tannic acid-crosslinked graphene oxide membranes for efficient treatment of oil contaminated water with enhanced stability, Heliyon 6 (10) (2020) e05127.
[29] B. Akkaya, B. Çakiroğlu, M. Özacar, Tannic Acid-Reduced Graphene Oxide Deposited with Pt Nanoparticles for Switchable Bioelectronics and Biosensors Based on Direct Electrochemistry, ACS Sustain Chem. Eng. 6 (2018) 3805–3814.
[30] Y. Fang, J.J. Tan, H. Choi, S. Lim, D.H. Kim, Highly sensitive naked eye detection of Iron (III) and H2O2 using poly-(tannic acid) (PTA) coated Au nanocomposite, Sens. Actuator B Chem. 259 (2018) 155–161.
[31] G. Yao, X. Liu, G. Zhang, Z. Han, H. Liu, Colloids Surf. A Physicochem. Eng. 625 (2021) 126972.
[32] C.-Y. Tang, P. Yu, L.-S. Tang, Q.-Y. Wang, R.-Y. Bao, Z.-Y. Liu, M.-B. Yang, W. Yang, Tannic acid functionalized graphene hydrogel for organic dye adsorption, Ecotoxicol. Environ. Saf. 165 (2018) 299–306.
[33] M.R. Muda, M.M. Ramli, S.S. Mat Isa, M.F. Jamlos, S.A.Z. Murad, Z. Norhanisah, M. Mohamad Isa, S.R. Kasjoo, N. Ahmad, N.I.M. Nor, N. Khalid, Fundamental study of reduction graphene oxide by sodium borohydride for gas sensor, AIP Conference Proceedings 1808 (2017) 020034.
[34] S. Badrayyana, D.K. Bhat, Novel one-pot green synthesis of graphene in aqueous medium under microwave irradiation using a regenerative catalyst and the study of its electrochemical properties, New J. Chem. 39 (2014) 420–430.
[35] S. Peng, C. Liu, X. Fan, Surface Modification of Graphene Oxide by Carboxyl-Group: Preparation, Characterization, and Application for Proteins Immobilization, Integrated Ferroelectrics 163 (2015) 42–53.
[36] T. Szabó, E. Tombácz, E. Illés, I. Dékány, Enhanced acidity and pH-dependent surface charge characterization of successively oxidized graphite oxides, Carbon 44 (3) (2006) 537–545.
[37] N.I.M. Nawi, S. Ong Amat, M.R. Bilad, N.A.H.M. Nordin, N. Shamsuddin, S. Prayogi, T. Narkkun, K. Faungnawakij, Development of Polyvinylidene Fluoride Membrane via Assembly of Tannic Acid and Polyvinylpyrrolidone for Filtration of Oil/Water Emulsion, Polymers 13 (6) (2021) 976.
[38] M. Mahkam, L. Doostie, The Relation Between Swelling Properties and Cross-Linking of Hydrogels Designed for Colon Specific Drug Delivery, Drug Deliv. 12 (2005) 343–347.
[39] A.V. Delgado, S. Ahualli, M.M. Fernández, M.A. González, G.R. Iglesias, J.F. Vivo-Vilches, M.L. Jimenez, Geometrical properties of materials for energy production by salinity exchange, Environmental Chemistry 14 (5) (2017) 279–287.
[40] L.-C. Xu, C.A. Siedlecki, Effects of surface wettability and contact time on protein adhesion to biomaterial surfaces, Biomaterials 28 (2007) 3273–3283.
[41] K. Menzies, L. Jones, The Impact of Contact Angle on the Biocompatibility of Biomaterials, Optom Vis Sci 87 (2010) 387–399.
[42] V.V. Neklyudov, N.R. Khafizov, I.A. Sedov, A.M. Dimiev, New insights into the solubility of graphene oxide in water and alcohols, Phys. Chem. Chem. Phys. 19 (2017) 17000–17008.
[43] D. Konios, M.M. Stylianakis, E. Stratakis, E. Kymakis, Dispersion behaviour of graphene oxide and reduced graphene oxide, J. Colloid Interface Sci. 430 (2014) 108–112.
[44] S. Wang, Y. Zhang, N. Abidi, L. Cabrales, Wettability and Surface Free Energy of Graphene Films, Langmuir 25 (2009) 11078–11081.
[45] D. Lin-Ven, N.B. Colthup, W.G. Fateley, J.G. Grasselli, The Handbook of Infrared and Raman Characteristic Frequencies of Organic Molecules, 1st ed.,., Academic Press, 1991, pp. 155–225.
[46] M.A. Pantoja-Castro, H. González-Rodríguez, Study by infrared spectroscopy and thermogravimetric analysis of tannins and tannic acid, Rev. Latinoam. Quim. 39 (2011) 107–112.
[47] D. Li, W. Zhang, X. Yu, Z. Wang, Z. Su, G. Wei, When biomolecules meet graphene: from molecular level interactions to material design and applications, Nanoscale 8 (2016) 19491–19509.
[48] H. Neuvonen, K. Neuvonen, A. Koch, E. Kleinpeter, P. Pasanen, Electron-Withdrawing Substituents Decrease the Electrophilicity of the Carbonyl Carbon. An Investigation with the Aid of 13C NMR Chemical Shifts, ν(CO) Frequency Values, Charge Densities, and Isodesmic Reactions To Interprete Substituent Effects on Reactivity, J. *Org. Chem.* 67 (2002) 6995–7003.
[49] H. Neuvonen, K. Neuvonen, P. Pasanen, Evidence of Substituent-Induced Electronic Interplay. Effect of the Remote Aromatic Ring Substituent of Phenyl Benzoates on the Sensitivity of the Carbonyl Unit to Electronic Effects of Phenyl or Benzoyl Ring Substituents, J. Org. Chem. 69 (11) (2004) 3794–3800.
[50] V. Nummert, O. Travnikova, S. Vahur, I. Leito, M. Piirsalu, V. Mäemets, I. Koppel, I.A. Koppel, Influence of substituents on the infrared stretching frequencies of carbonyl group in esters of benzoic acid, J. Phys. Org. Chem. 19 (10) (2006) 654–663.
[51] A.M. Diez-Pascual, M. Naffakh, Grafting of an aminated poly(phenylene sulphide) derivative to functionalized single-walled carbon nanotubes, Carbon 50 (2015) 857–868.
[52] S.W. Chong, C.W. Lai, S.B.A. Hamid, Green preparation of reduced graphene oxide using a natural reducing agent, Ceramics International 41 (8) (2015) 9505–9513.
[53] A.M. Diez Pascual, C. Vallés, R. Mateos, S. Vera-López, I.A. Kinloch, M.P. San Andrés, Influence of surfactants of different nature and chain length on the morphology, thermal stability and sheet resistance of graphene, Soft Matter 14 (2018) 6013–6023.
[54] D.R. Pompeu, Y. Larondelle, H. Rogez, O. Abbas, J.A.F. Pierna, V. Baeten, Characterization and discrimination of phenolic compounds using Fourier transform Raman spectroscopy and chemometric tools, Biotechnol., Agron., Soc. Environ. 22 (2018) 13–28.
[55] M. Labieniec, T. Gabryelak, Interactions of tannic acid and its derivatives (ellagic and gallic acid) with calf thymus DNA and bovine serum albumin using spectroscopic method, J. Photochemistry Photobiology B: Biology 82 (1) (2006) 72–78.
[56] C.-C. Hsueh, C.-C. Wu, B.-Y. Chen, Polyphenolic compounds as electron shuttles for sustainable energy utilization, Biotechnol Biofuels 12 (2019) 271.
[57] A. Das, B. Chakraborty, A.K. Sood, Raman Spectroscopy of graphene on different substrates and influence of defects, Bull. Mater. Sci. 31 (3) (2008) 579–584.
[58] D. Lopez-Díaz, M.L. Holgado, J.L. García-Fierro, M.M. Velazquez, Evolution of the Raman Spectrum with the Chemical Composition of Graphene Oxide, J. Phys. Chem. C 121 (2017) 20489–20497.
[59] A.A.K. King, B.R. Davies, N. Noorbehesht, P. Newman, T.L. Church, A.T. Harris, J. M. Razal, A.I. Minett, A New Raman Metric for the Characterisation of Graphene Oxide and Its Derivatives, Sci. Rep. 6 (2016) 19491.
[60] A.C. Ferrari, J. Robertson, Interpretation of Raman Spectra of Disordered and Amorphous Carbon, Phys. Rev. B: Condens. Matter Mater. Phys. 61 (2000) 14095–14107.
[61] M. Ilčíková, M. Mrlík, Z. Spitalsky, M. Micusik, K. Csomorová, V. Sasinkova, A. Kleinova, J. Mosnacek, A tertiary amine in two competitive processes: Reduction of graphene oxide vs. catalysis of atom transfer radical polymerization, RSC Adv. 5 (2015) 3370–3376.
[62] C. Vallés, D.G. Papageorgiou, F. Lin, Z. Li, B.F. Spencer, R.J. Young, I.A. Kinloch, PMMA-grafted graphene nanoplatelets to reinforce the mechanical and thermal properties of PMMA composites, Carbon 157 (2020) 750–760.
[63] D. Zhang, S. Yang, Y. Chen, S. Liu, H. Zhao, J. Gu, ^{60}Co γ-ray Irradiation Crosslinking of Chitosan/Graphene Oxide Composite Film: Swelling, Thermal Stability, Mechanical, and Antibacterial Properties, Polymers 10 (3) (2018) 294.
[64] H. Dai, Y. Chen, S. Zhang, X. Feng, B. Cui, L. Ma, Y. Zhang, Enhanced Interface Properties and Stability of Lignocellulose Nanocrystals Stabilized Pickering Emulsions: The Leading Role of Tannic Acid, J. Agric. Food Chem. 69 (48) (2021) 14650–14661.
[65] F. Yang, J. Yang, S. Qiu, W. Xu, Y. Wang, Tannic acid enhanced the physical and oxidative stability of chitin particles stabilized oil in water emulsion, Food Chem. 346 (2021) 128762.
[66] G. Vogt, P. Argos, Protein thermal stability: hydrogen bonds or internal packing?, Folding and Design 2 (4) (1997) S40–S46
[67] M. Tsakos, E.S. Schaffert, L.L. Clement, N.L. Villadsena, T.B. Poulsena, Ester Coupling Reactions– an Enduring Challenge in the Chemical Synthesis of Bioactive Natural Products, Nat. Prod. Rep. 32 (2015) 605–632.
[68] Y. Wang, H.F. Zhan, Y. Xiang, C. Yang, C.M. Wang, Y.Y. Zhang, Effect of Covalent Functionalization on Thermal Transport across Graphene-Polymer Interfaces, J. Phys. Chem. C 119 (22) (2015) 12731–12738.
[69] L. Fouad, K. Valeriia, L. Costes, S. Brohez, R. Mincheva, P. Dubois, Novel Bio-based Flame Retardant Systems Derived from Tannic Acid, J. Renew. Mater. 6 (6) (2015) 559–572.
[70] X. Chen, X. Xi, A. Pizzi, E. Fredon, X. Zhou, J. Li, C. Gerardin, G. Du, Preparation and Characterization of Condensed Tannin Non-Isocyanate Polyurethane (NIPU) Rigid Foams by Ambient Temperature Blowing, Polymers 12 (4) (2020) 750.
[71] S. Basak, A.S.M. Raja, S. Saxena, P.G. Patil, Tannin based polyphenolic bio-macromolecules: Creating a new era towards sustainable flame retardancy of polymers, Polymer Degradation and Stability 189 (2021) 109603.
[72] O. Akhavan, E. Ghaderi, Toxicity of Graphene and Graphene Oxide Nanowalls Against Bacteria, ACS Nano 4 (2010) 5731–5736.
[73] A.M. Díez-Pascual, J.A. Luceño-Sánchez, Antibacterial Activity of Polymer Nanocomposites Incorporating Graphene and Its Derivatives: A State of Art, Polymers 13 (2021) 2105.
[74] A.M. Díez-Pascual, State of the Art in the Antibacterial and Antiviral Applications of Carbon-Based Polymeric Nanocomposites, Int. J. Mol. Sci. 22 (2021) 10511.
[75] B. Kaczmarek, Tannic Acid with Antiviral and Antibacterial Activity as A Promising Component of Biomaterials-A Minireview, Materials. 13 (14) (2020) 3224.
[76] G. Dong, H. Liu, X. Yu, X. Zhang, H. Lu, T. Zhou, J. Cao, Antimicrobial and anti-biofilm activity of tannic acid against Staphylococcus aureus, Natur. Product Res. 32 (18) (2018) 2225–2228.
[77] A. Dabbaghi, K. Kabiri, A. Ramazani, M.J. Zohuriaan-Mehr, A. Jahandideh, Synthesis of bio-based internal and external cross-linkers based on tannic acid for preparation of antibacterial superabsorbents, Polym. Adv. Technol. 30 (11) (2019) 2894–2905.